Journal of Visualization, Vol. 5, No. 3 (2002) 273-283

Flow Morphologies of Two Shock-accelerated Unstable Gas Cylinders

Tomkins, C.*1, Prestridge, K.*1, Rightley, P.*1, Vorobieff, P.*2 and Benjamin, R.*1

*1 Dynamic Experimentation Division, Los Alamos National Laboratory, Los Alamos, NM87545, USA.
*2 Department of Mechanical Engineering, University of New Mexico, Albuquerque, NM87131, USA.

Received 17 November 2001.
Revised 8 March 2002.

***Abstract*:** Our highly reproducible shock-tube experiments examine the interaction of two unstable, compressible gas cylinders accelerated by a planar shock wave. Flow visualization shows that the evolution of the double-cylinder flow morphologies is dominated by two counter-rotating vortex pairs, the strength and behavior of which are observed to be highly sensitive to the initial cylinder separation. Simulations of the flow based on idealized vortex dynamics predict grossly different morphologies than those observed experimentally, suggesting that interactions at early time weaken the inner vortices. A correlation-based ensemble averaging procedure permits decomposition of the concentration field into mean and fluctuating components, providing evidence that energy is transferred from the intermediate to the small scales at late time.

***Keywords*:** visualization, Richtmyer-Meshkov instability, shock wave, vortex dynamics.

1. Introduction

The Richtmyer-Meshkov (RM) instability (Meshkov, 1969) occurs during the impulsive acceleration of a perturbed interface between two materials of different density, as the misalignment of the density gradient and pressure gradient leads to a baroclinic production of vorticity. RM instability plays an important role in several areas, ranging from inertial confinement fusion to the evolution of supernovae, but the complexity of the resulting vortex-dominated flow often makes the prediction of fundamental late-time behavior, such as the degree of mixing, difficult.

One simple test problem for the study of the RM instability is the interaction of a shock wave with a compressible gas cylinder. This problem has been examined theoretically (Samtaney and Zabusky, 1994) and computationally (Zoldi, 2002) in two dimensions, and experimentally with nominally two-dimensional initial conditions (Jacobs, 1993; Prestridge et al., 2001). The Prestridge study considers a Mach 1.2 shock propagating through air and interacting with a heavy-gas (SF_6) cylinder. The cylinder interface becomes RM-unstable, initially growing linearly, and then quickly transitioning to a non-linear regime in which the baroclinically-deposited vorticity rolls up into two dominant counter-rotating vortices. At later times, a secondary instability sets in (possibly Kelvin-Helmholtz, or possibly baroclinic (Cook and Miller, 2001)), which causes the breakdown of the flow structures into smaller scales, and initiates the transition to turbulence. This gas-cylinder problem has also proven valuable for code validation; it possesses a simple initial configuration, but exhibits complex, non-linear behavior (Prestridge et al., 2001).

In the present work, we perform an experimental investigation of the pre-turbulent instability created by the interaction of a planar shock with two heavy-gas (SF_6) cylinders surrounded by air. The cylinders are initially separated spanwise, become RM-unstable upon shock impact, and then interact as they convect downstream. The

degree of interaction is varied by adjusting the initial center-to-center spanwise spacing of the cylinders from 1.2 to 2.0 times the cylinder diameter, nominally. The post-shock evolution of the system is captured at six times using laser visualization, including the primary interfacial instability, the non-linear interaction of baroclinically-generated vortices, and the onset of secondary instabilities.

The double-cylinder configuration, like the single-cylinder case, provides an interesting base problem for study of the RM instability, and subsequent transition to turbulence. In addition, aspects of vortex dynamics become important in the flow evolution, e.g., vortex column interactions. The double-cylinder problem also provides a highly challenging test for computationalists, again despite a relatively simple initial configuration, not only due to the non-linearity inherent in the RM instability, but also due to a particularly keen sensitivity to initial conditions. It is observed that different initial separations lead to flow solutions that not only differ greatly with respect to resulting flow morphology, but may also differ in terms of the dominant mechanisms of interaction. Hence, one simple initial geometry may provide more than one code validation problem - each problem emphasizing different aspects of physics - simply by altering the initial cylinder separation.

2. Experimental Details

2.1 Shock Tube

A side-view schematic of the shock tube is presented in Fig. 1. The shock is generated by placing a diaphragm at the downstream end of the driver section, and pressurizing the section to approximately 20 psi. Solenoid-driven blades puncture the diaphragm, releasing a Mach 1.2 shock in air, which becomes planar as it propagates through the driven section and impacts one or two heavy-gas cylinders in the test section. The heavy gas is sulfur hexaflouride, SF_6, with a density five times that of air. The tube cross-section is 75×75 mm.

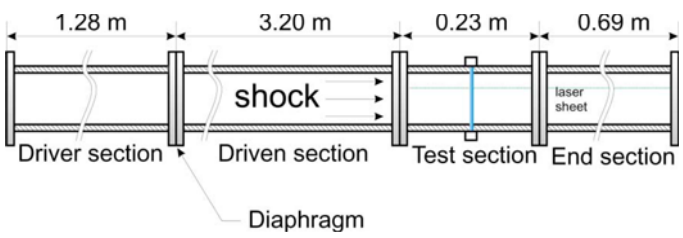

Fig. 1. Schematic of shock tube.

A schematic of the test section is shown in Fig. 2. The gas cylinders are created as follows. Heavy gas is fed into a container that is elevated above the test section. Glycol/water fog droplets (nominally 0.5-1.0 μm in diameter, created with a commercial theatrical fog generator) are well mixed with the gas, and the combination is allowed to flow into the test section driven by gravity and mild suction. Theoretical and experimental analyses confirming the flow-tracking fidelity of the droplets were performed by Rightley et al. (1997, 1999) and Prestridge et al. (2000), including comparisons with direct Rayleigh scattering from the SF_6 without fog present. The geometry of the gas-fog mixture in the test section thus depends upon the shape of the output orifice, which in the present experiment is either one nozzle of circular cross-section (to create a single vertical gas cylinder) or two circular nozzles separated spanwise (to create two gas cylinders, as depicted in Fig. 2). The vertical flow velocity ($\approx$ 20 cm/s) is negligible in comparison with the speed of the shock or the convection velocity of the unstable flow structures ($\approx$ 100 m/s). The flow system is modular in that the sections containing the nozzles may be interchanged. Thus, one insert is machined for each geometry, and the configuration of gas is changed by simply switching inserts; in this way, the center-to-center spacing S of the cylinders is carefully controlled and adjusted in a repeatable fashion. Each insert is designed to produce a smooth, laminar flow, and observations of the flowing gas reveal steady, two-dimensional cylinders with smooth edges. A more rigorous test of the repeatability and control of the initial conditions (ICs), however, is provided by the images themselves. Statistical analysis of the images shows high repeatability from shot to shot for each initial spacing on the scales associated with the initial geometry and the primary interfacial instability. Due to the sensitivity of the flow evolution to the initial gas configuration, this repeatability provides quite rigorous corroboration that the ICs are well-controlled.

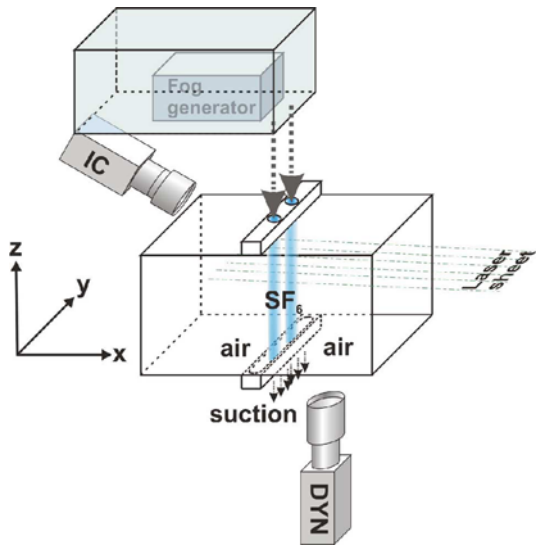

Fig. 2. Schematic of shock tube test section.

A top-view cross-section of the double-cylinder configuration immediately before shock impact is shown schematically in Fig. 3. In the present work, experiments are conducted at S/D = 1.2, 1.4, 1.5, 1.6, 1.8 and 2.0, nominally, where D is the cylinder diameter (here $D \approx 3.1$ mm), although the true spacing may be slightly different from the nominal spacing. An additional set of experiments is performed for the case of a single cylinder, for comparison. Approximately 15 realizations are captured at each initial separation.

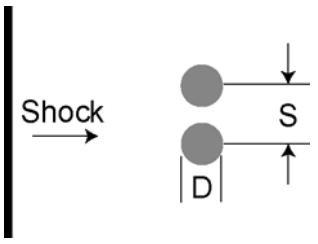

Fig. 3. Schematic of double-cylinder configuration. The initial spanwise center-to-center separation S ranges from 1.2D to 2.0D, where D is the cylinder diameter.

2.2 Diagnostics

The flow is illuminated with a custom Nd:YAG laser that provides 7 pulses, each approximately 10 ns in duration, spaced 140 μs apart. The beam is spread to form a horizontal sheet in the test section, parallel with the tube floor (as depicted in Fig. 1), and is focused down in the vertical direction to approximately 1 mm in thickness. Optical access for the beam is provided by a glass window in the tube end section. The timing of the laser (and cameras) relies on a pressure transducer located in the shock tube wall directly upstream of the test section. The laser is timed to provide one pulse immediately before shock impact, to illuminate the initial condition, and six pulses during the post-shock flow evolution, before the unstable gas convects out of the test section. All data are acquired before the shock reflected from the test section end or the rarefraction from the driver section reach the test section. The initial conditions are captured with a Photometrics 512 × 512 CCD camera, labeled "IC" in Fig. 2, which is tilted at 45 degrees to the light sheet. The image of the initial conditions is remapped to compensate for the combination of the resulting distortion and the "fish-eye" effect produced by the IC lens. The mapping procedure uses bicubic splines. The mapping coefficients are determined by acquiring a distorted image of a test grid, and comparing with the same grid undistorted. The light scattered from the gas during the six post-shock (or "dynamic") laser pulses is captured with a Hadland Photonics SVR 1134 × 486 intensified camera, labeled "DYN" in Fig. 2, which is aligned normal to the light sheet. This camera does not image individual particles, but collects images of local particle concentration, which in the post-shock flow is proportional to the local density (Prestridge

et al., 2000). Because the structure is convecting at approximately 100 m/s, the entire event (from the IC capture to the last dynamic pulse) takes less than 1 ms.

3. Results and Discussion

3.1 Single-Cylinder Flow Morphologies

Before considering the case of two shock-accelerated, interacting cylinders, let us first revisit the case of a shock wave impacting one heavy-gas cylinder. This problem has been previously examined experimentally (Jacobs, 1993; Prestridge et al., 2001) and computationally (Zoldi, 2002), but the experiment is repeated here in order to permit a fair comparison - i.e., with nearly identical conditions other than the number of cylinders - with the double-cylinder case. It will be seen from these measurements that in the single-cylinder case, the flow is dominated by two equal strength vortices and, with the exception of the small scales, the flow morphologies are symmetric about the spanwise midplane (i.e., the *x*-*z* plane that bisects the vortex pair).

An example of the single-cylinder density-field evolution is presented in Fig. 4. Here the flow is from left to right, and the leftmost image represents the (initial) conditions immediately before shock impact. Note that in this and subsequent figures the intensity level of the initial conditions (t = 0 ms) is lower than that of the dynamic images. This is simply because a different (non-intensified) camera was used for the IC acquisition. The six subsequent images, moving left to right, are acquired at t = 50, 190, 330, 470, 610 and 750 ms after shock impact, respectively. Differences in total intensity in these post-shock images are due to variability in the energy of the laser pulses.

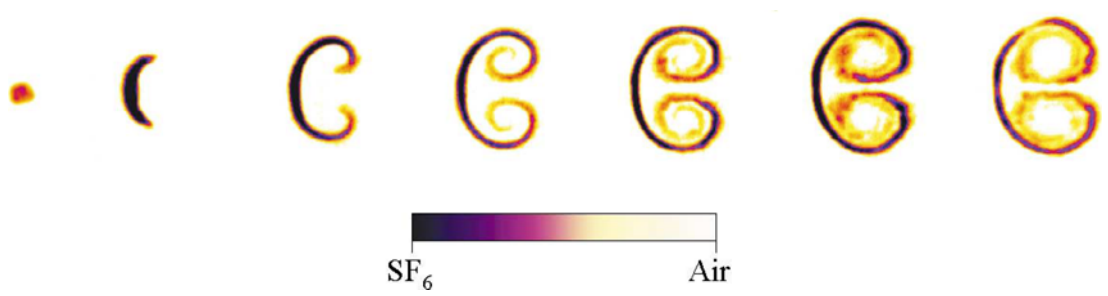

Fig. 4. False-color flow morphologies of a single shock-accelerated gas cylinder at t = 0, 50, 190, 330, 470, 610 and 750 ms, respectively, after shock impact. Shock and flow are left to right.

The baroclinic vorticity deposited by the shock along the air-SF_6 interface rolls up into a pair of counter-rotating vortices, and entrains the fog-seeded dense gas around the vortex cores. Note also the presence of waviness along the interface within the vortex cores, appearing first at t = 470 ms, and evident at later times as well. This waviness is interpreted as a manifestation of a secondary instability that occurs along the gaseous interface. The physics of the single-cylinder case are discussed in more detail in Prestridge et al. (2001). For the moment, however, it is sufficient to note (for purposes of comparison) that the single-cylinder morphologies are dominated by two equal strength vortices, and the flow is symmetric about the spanwise midplane on all but the smallest scales.

3.2 Double-Cylinder Vortex Blob Simulation

We now turn our attention to the focus of the present paper: flow morphologies resulting from the interaction of two shock-accelerated, unstable gas cylinders. Before examining the experimental data, however, it is interesting to consider what one would expect to see based on idealized vortex dynamics. In this section, results from a "vortex blob" simulation (Nakamura et al., 1982; Rightley et al., 1997) will be presented, in which an initial distribution of idealized vortices is specified, and then the flow permitted to evolve in time. These vortices are defined as two-dimensional, axisymmetric "blobs" of vorticity with Gaussian cores. The evolution of the vortex system is observed by inserting massless "marker particles" in the simulation. This approach has been used effectively in simulating the evolution of a shock-accelerated gas curtain (Rightley et al., 1997). By specifying a row of counter-rotating vortices, the authors were able to quite accurately predict the integral growth rate of the

instability, and capture the gross flow morphology.

In Fig. 5, results are presented for a two-dimensional vortex blob simulation of the double-cylinder configuration with spanwise separation. The initial cylinder spacing is $S = 2.0D$, and marker particles are densely distributed within the heavy-gas cylinders (see Fig. 5(a)). The baroclinic vorticity deposition is simulated here by specifying two pairs of equal-strength, counter-rotating vortices, with one vortex on the upper and lower edge of each cylinder. The vortices are located along the streamwise midplane (i.e., the bisecting *y-z* plane) of the cylinders, which, in theory, are the areas of greatest baroclinic vorticity production.

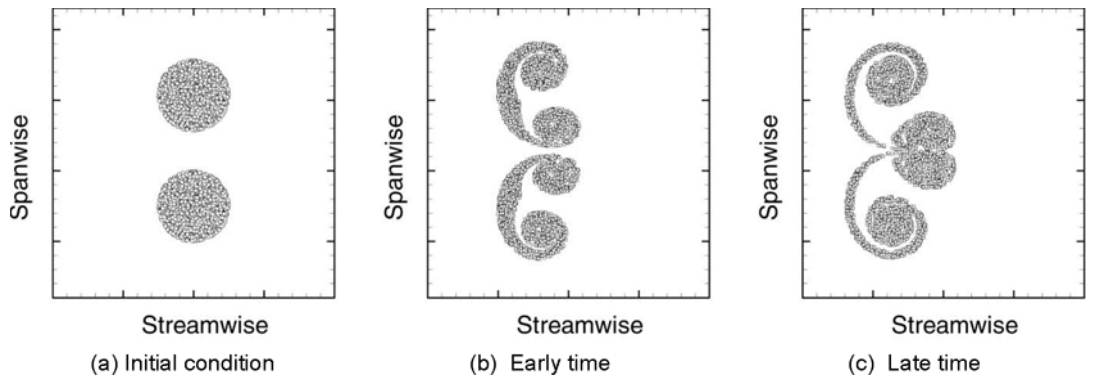

Fig. 5. Idealized vortex blob simulation of double-cylinder flow evolution with $S = 2.0D$.

The idealized evolution of the cylinders is presented in Figs. 5(b) and 5(c). These figures approximately correspond to early and late times in the flow evolution, respectively. In Fig. 5(b), each cylinder is observed to distort by the induction of the vortices, which entrain the heavy gas of the cylinders. Interestingly, the flow morphology looks qualitatively similar to two unstable single cylinders, as seen in the previous experimental example (which is dominated by a pair of counter-rotating vortices). One obvious difference in the double-cylinder simulation is that the vortex pairs are slightly rotated - an indication of interaction. In Fig. 5(c), the morphology begins to change significantly. The two inner vortices, also counter-rotating, move forward (downstream) relative to the outer vortices, due to mutual induction. They continue to entrain significant material, however. Thus, the vortex blob simulation suggests that significant interaction occurs between the two unstable cylinders, even with a relatively large ($S = 2.0D$) initial separation. Furthermore, preliminary computational results (Zoldi, 2001) with idealized initial conditions qualitatively agree with the vortex blob simulations, in terms of the large-scale flow morphologies.

3.3 Double-Cylinder Experimental Flow Morphologies

Flow morphologies are presented of the evolution of two interacting, RM-unstable, SF_6 cylinders in Figs. 6-8. Each image shows the initial conditions and six subsequent dynamic exposures. Experiments are performed at six values of the nominal, initial, spanwise, center-to-center separation: $S/D = 1.2$, 1.4, 1.5, 1.6, 1.8 and 2.0. The flow morphologies are separated into three groups, according to the degree of cylinder-cylinder interaction that appears to occur: weak interaction, moderate interaction and strong interaction (all described below). Two values of the initial separation S/D are associated with each group.

Examples of flow morphologies for the case of "weak interaction" are presented in Fig. 6. The initial cylinder separations are $S/D = 2.0$ (Fig. 6(a)) and $S/D = 1.8$ (Fig. 6(b)). In these cases, the resulting flow structures look qualitatively similar to a pair of uncoupled single-cylinder realizations. In particular, two counter-rotating vortices per cylinder are observed to develop. The obvious differences between these structures and the ones in the single-cylinder case are in the rotation and trajectory of the structures: in the two-cylinder case, the vortex pairs are rotated so that the outer vortices are downstream, and the trajectories of the structures are altered, so that the centers of mass slightly separate over time.

Fig. 6. Examples of double-cylinder flow morphologies: weak interaction. Images are acquired at t = 0, 50, 190, 330, 470, 610 and 750 μs after shock impact. Legend as in Fig. 4. (a) $S = 2.0D$; (b) $S = 1.8D$.

Note that the morphologies presented in Fig. 6(a) are significantly different, particularly at late time, from the structures predicted by the vortex blob simulation, which also assumes S/D = 2.0 for the initial condition. In the experiment, the baroclinically-deposited vorticity around each cylinder rolls up into a pair of counter-rotating vortices, in agreement with the simulation; however, the evolution of the flow structures, controlled by the induction of these vortices, is clearly different. While the simulated inner vortices are mutually induced downstream, the inner vortices in the experiment are induced upstream (relative to the outer ones). The motion of the simulated vortices is consistent with the motion of point vortices, of equal strength, in a plane. The motion of the vortices in the experiment, however, is clearly inconsistent with the motion of idealized vortices of equal strength - but it would be consistent with idealized vortex dynamics if the outer vortices were significantly stronger than the inner vortices. In this case, the outer vortices could induce the inner vortices upstream - as is the case in Figs. 6(a) and 6(b). In this interpretation, then, the presence of a second cylinder leads to an interaction that alters the relative strength of the inner and outer vortices. To evaluate the validity of this hypothesis, let us consider initial configurations that lead to a greater degree of cylinder-cylinder interaction.

Flow morphologies for initial spacings that lead to "moderate interaction" are presented in Fig. 7. In these examples, S/D = 1.6 and 1.5. The degree of interaction in these cases is labeled "moderate" because two counter-rotating vortices still form per cylinder, although now the inner vortices are severely retarded in their formation. Hence, the actual morphologies are being significantly altered in addition to the rate of rotation and/or trajectory of the structures. Note that in Fig. 7(a), with S/D = 1.6, the inner vortices appear to have induced a slight rollup of the heavy gas, while in Fig. 7(b), with S/D = 1.5, the heavy gas around the inner vortices appears to have simply formed two circles (or columns in three dimensions). It should be emphasized that the morphologies presented here, and for all other initial separations, are representative of the ensemble of data for a given separation, again due to the repeatability of the experiment. Thus, only one example is necessary per dataset.

The morphologies in Fig. 7 also support the earlier hypothesis that the rotation of the structures is due to a difference in the strength of the inner and outer vortices. Indeed, the inner vortices are clearly underdeveloped, and the rate of rotation for both S/D = 1.6 and 1.5 is greater than for the weak interaction case. Thus the outer vortices, now dominant, appear to be inducing the inner ones around them. To gain a full understanding of the evolution, however, we must also understand why the inner vortices are weak relative to the outer ones, or, more specifically: what type of interaction(s) is occurring that affects the formation or development of these vortices. One possibility is vorticity cancellation (or vortex annihilation) between the inner structures shortly after shock passage, so that the remaining inner vortices are weakened, and more severely with increased interaction, i.e., decreasing initial

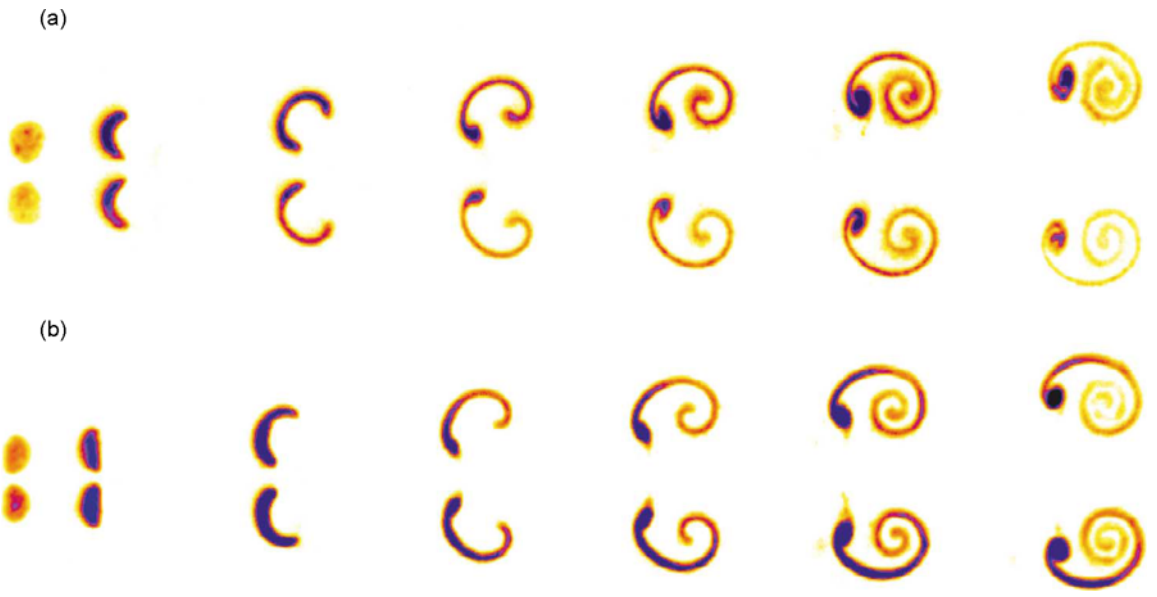

Fig. 7. Examples of double-cylinder flow morphologies: moderate interaction. Images are acquired at t = 0, 50, 190, 330, 470, 610 and 750 ms after shock impact. Legend as in Fig. 4. (a) $S = 1.6D$; (b) $S = 1.5D$.

Fig. 8. Examples of double-cylinder flow morphologies: strong interaction. Images are acquired at t = 0, 50, 190, 330, 470, 610 and 750 ms after shock impact. Legend as in Fig. 4. (a) $S = 1.4D$; (b) $S = 1.2D$.

separation. Another possibility is that the addition of a second cylinder in close proximity to the first affects the shock-cylinder interaction, and thus alters the initial baroclinic vorticity deposition. A third possibility, of course, is that both types of interactions are taking place to one degree or another. Unfortunately, it is not possible to unequivocally answer this question with the current data, and simulations have yet to provide any insights.

Examples of flow morphologies for the "strong interaction" case are presented in Fig. 8. The initial cylinder separation is now reduced to S/D = 1.4 and 1.2. The degree of interaction is labeled "strong" here because the flow structures are fundamentally altered, as the inner vortices either do not form or are completely annihilated shortly after formation. The flow evolution is thus completely dominated by the outer vortices. In fact, as the separation is reduced to its smallest value as in Fig. 8(b), the morphologies appear qualitatively similar to the single-cylinder case (Fig. 4). Note even the emergence of a secondary instability at later times, as seen in the single-cylinder data.

The foregoing results and interpretation clearly reveal interesting and complex behavior, including a strong sensitivity of the cylinder-cylinder interaction and resulting flow morphology to the initial cylinder separation. The most striking example of this sensitivity is an apparent bifurcation point in the flow evolution - the branches of which correspond to the eventual development of 2 or 4 vortices - that occurs between S/D = 1.4 and 1.5. Thus, altering the initial separation by only approximately 7% (310 mm) leads to quite different solutions - truly non-linear behavior. The present problem is also interesting from a code validation standpoint. Although it employs a relatively simple initial configuration, the behavior is clearly non-linear in terms of the separation, and the resulting flow morphologies prove to be quite complex. Furthermore, by simply changing the initial cylinder separation, one can emphasize (or seek to validate) different physics. For example, the S/D = 1.2 case would more rigorously test shock-cylinder interactions, and the S/D = 2.0 case would emphasize post-shock vortex dynamics.

3.4 Fluctuating Intensity Fields

The results and discussion thus far have focused on the largest scales (i.e., the length and width of the structure) and the intermediate scales (i.e., the rollup within the vortices) of the flow. It is also of interest, however, to examine the smaller flow scales, which are important in mixing. In the following section we briefly describe an iterative correlation-based ensemble averaging technique that permits decomposition of the concentration fields into mean and fluctuating components. Selected fluctuating fields are also presented, which readily reveal the behavior of the small scales.

It is desirable to perform ensemble averaging for both quantitative and qualitative analysis. Two aspects of the current experiment, however, make the ensemble averaging procedure difficult: first, the sensitivity of the flow evolution to the initial conditions, as discussed in the previous subsection, and second, a slight jitter in the timing between the shock passing the pressure transducer and the firing of the lasers, resulting in a slight jitter in the location of the flow structures on the CCD array. Hence, it is desirable to remove this spatial "jitter" before averaging, to ensure that the average, and any subsequent decomposition based on the average, is meaningful. The procedure used to perform the ensemble averaging is outlined only briefly here - a more thorough description is given by Tomkins et al. (2002).

First, the multi-exposure images are separated into sections, to yield one exposure (or time of evolution) per image (i.e., section). Then all of the images for a given initial cylinder separation and time are grouped together and analyzed using a template-matching scheme (see, for example, Soloff, 1997). One image is selected from the group, used as an initial "template" and matched - using a spatial correlation - to each of the other images or "fields." (A field is simply the region to which a template is matched; in this case, an image.) The region of each field around the maximum correlation is extracted, and these regions are ensemble averaged. The result of this ensemble averaging procedure is then used as the template for the next iteration, and the ensemble average of all of these 2nd-iteration extracted regions is the final ensemble average. Thus, there is one ensemble-averaged result for each initial cylinder spacing and each laser pulse, and the spatial jitter present between realizations is removed, permitting a meaningful ensemble average. An additional advantage of the procedure is that the regions extracted from the original (i.e., total) fields are already matched spatially with the average field; thus, the fluctuating field is easily obtained by subtracting the average field from the total field.

The results from the correlation-based ensemble averaging procedure for $S = 1.2D$ are presented in Fig. 9. Included are all six dynamic images and the initial conditions. It can be seen from Fig. 9 that both the largest scales and the intermediate scales of the flow have persisted through the ensemble average. The persistence of this structure strongly suggests that the ensemble averaging procedure is successful in removing the spatial jitter between realizations, and in capturing the "average" character of the unstable cylinder morphologies. Furthermore, and just as importantly, it is a testament to the repeatability of the data.

Fig. 9. Correlation-based ensemble-averaged flow morphology for $S = 1.2D$. Acquisition times and legend as in previous figures.

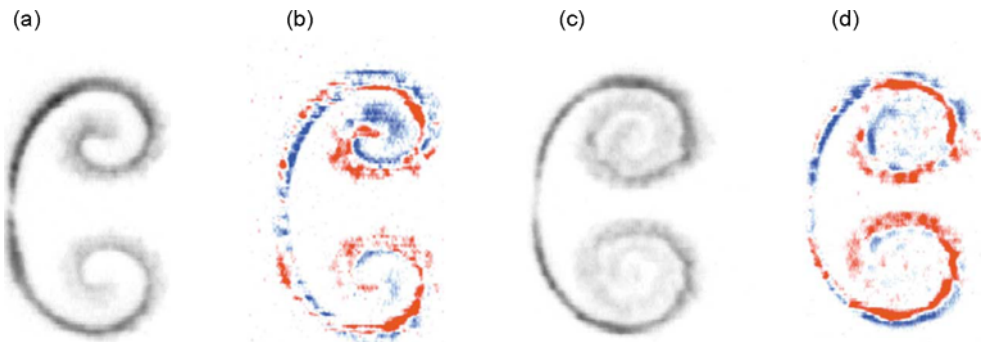

Fig. 10. Total and fluctuating intensity (concentration) fields with $S = 1.2D$. Fluctuating fields are colorized to distinguish positive (red) from negative (blue) concentration fluctuations. (a) Total field, $t = 470$ ms; (b) fluctuating field, $t = 470$ ms; (c) total field, $t = 750$ ms; (d) fluctuating field, $t = 750$ ms.

Examples of total (i.e., instantaneous) and fluctuating concentration fields are shown in Fig. 10. Figures 10(a) and 10(b) are the total and fluctuating fields, respectively, at $t = 470$ ms after shock impact with $S = 1.2D$. Figures 10(c) and 10(d) are the total and fluctuating fields at $t = 750$ ms after shock impact. Figures 10(b) and 10(d) are brightened to emphasize the fluctuations, and colorized to distinguish the positive fluctuations (red) from the negative ones (blue). Inspection of Fig. 10 reveals that the fluctuating fields bring out the character of the small scales. In particular, the emergence and character of a secondary instability, which develops along the air-SF_6 interface within (and on the edges of) the vortex cores (Prestridge et al., 2001), is more readily revealed by the decomposition. As discussed earlier, the instability is manifest as waviness along the interface, which is typically evident along the outer edges of the vortex cores as in Fig. 10(c). Of course the instability is also manifest in the corresponding fluctuating field, Fig. 10(d), as waviness or discontinuity in the regions of positive or negative concentration fluctuations. At earlier time, however, the appearance of the instability may not be obvious in the total field - as in Fig. 10(a). The beginning stages of the instability, however, are revealed in Fig. 10(b), again as waviness or discontinuity in the fluctuations, most obviously the positive (red) fluctuations.

This decomposition also makes evident another event, or series of events, associated with instability and the transition process: the breakdown of intermediate scales to small scales within the vortex cores. Inspection of Fig. 10(b) ($t = 470$ ms) reveals relatively large regions of contiguous positive and negative fluctuations within the vortex cores, particularly within the upper vortex. These large regions of fluctuation suggest that the intermediate flow scales are intact within the vortex. The cores of the vortices in Fig. 10(d) ($t = 750$ ms), however, contain almost no large-scale fluctuations, only a series of weak and small-scale positive and negative fluctuations. This change in the nature of the fluctuations is consistent with the transfer of energy from the intermediate (rollup) scales of the flow to the smaller scales, on which mixing occurs.

4. Conclusions

We use flow visualization to experimentally investigate the evolution of two interacting, RM-unstable gas cylinders. Flow morphologies for a range of initial cylinder spacings are captured at six times after shock passage, with high repeatability, and are compared with the case of a single shock-accelerated cylinder and simulations. The degree of cylinder-cylinder interaction, and hence the resulting flow morphology, is observed to be highly sensitive to the initial cylinder spacing. The data are classified into three groups based on this degree of interaction: those separations that lead to weak interaction (manifest as a rotation of vortex pairs), moderate interaction (resulting in an alteration of morphology) and strong interaction (in which case no inner vortices appear to form). An apparent bifurcation point is also observed between $S/D = 1.4$ and 1.5, the branches of which correspond to the post-shock formation of two and four vortices.

Vortex blob simulations of a weak interaction case based on idealized vortex dynamics with equal strength vortices predict quite different flow morphologies from those observed experimentally. This discrepancy suggests that interactions weaken the inner vortices, either by affecting the initial baroclinic vorticity deposition, or due to a post-shock vortex annihilation process, so that the outer vortices induce the inner vortices upstream and outwards.

A correlation-based ensemble averaging procedure effectively captures both the large and intermediate scales of the flow, providing confirmation of the experimental repeatability and permitting decomposition of the concentration field into mean and fluctuating components. The fluctuating fields more readily reveal smaller-scale phenomena, including the emergence of a secondary instability along the air-SF_6 interface, and the breakdown of intermediate flow scales to smaller (mixing) scales at late time within the vortex cores.

Acknowledgments

The authors would like to thank James Doyle, Randall Johnson, Norman Kurnit and Michael Schneider for technical assistance, and Charles Cranfill, James Kamm, Mark Marr-Lyon and Cindy Zoldi for suggestions on this manuscript. This work was supported by DOE contract W-7405-ENG-36 and Sandia Laboratories Grant BG-7553.

References

Baltrusaitis, R., Gittings, M., Weaver, R., Benjamin, R. and Budzinski, J., Simulation of Shock-generated Instabilities, Phys. Fluids, 8 (1996), 2471.

Cook, A. and Miller, P., Personal Communication, (2001).

Jacobs, J., The Dynamics of Shock-accelerated Light and Heavy Gas Cylinders, Phys. Fluids A, 5-9 (1993), 2239.

Meshkov, E., Instability of the Interface of Two Gases Accelerated by a Shock Wave, Izv. Akad. Nauk. SSSR Mekh. Zhidk. Gaza., 4 (1969), 151.

Nakamura, Y., Leonard, A. and Spalart, P., Vortex Simulation of an Inviscid Shear Layer, AIAA Paper No. 82-0948 (1982).

Prestridge, K., Rightley, P. M., Vorobieff, P., Benjamin, R. F. and Kurnit, N. A., Simultaneous Density-field Visualization and PIV of a Shock-accelerated Gas Curtain, Exp. Fluids, 29 (2000), 339.

Prestridge, K., Zoldi, C., Vorobieff, P., Rightley, P. and Benjamin, R., Experiments and Simulations of Instabilities in a Shock-accelerated Gas Cylinder, Los Alamos National Laboratory Report No. LAUR-00-3973 (2001).

Rightley, P., Vorobieff, P. and Benjamin, R., Evolution of a Shock-accelerated Thin Fluid Layer, Phys. Fluids, 9-6 (1997), 1770.

Rightley, P., Vorobieff, P., Martin, R. and Benjamin, R., Experimental Observations of the Mixing Transition in a Shock-accelerated Gas Curtain, Phys. Fluids, 11-1 (1999), 186.

Samtaney, R. and Zabusky, N., Circulation Deposition on Shock-accelerated Planar and Curved Density-stratified Interfaces: Models and Scaling Laws, J. Fluid Mech., 269 (1994), 45.

Soloff, S., An Investigation of the Small-scale Structure in a Turbulent Pipe Flow Using High Resolution Particle Image Velocimetry, M.S. thesis, Department of Theoretical and Applied Mechanics, University of Illinois at Urbana-Champaign, (1997).

Tomkins, C., Prestridge, K., Rightley, P., Marr-Lyon, M., Vorobieff, P. and Benjamin, R., A Quantitative Investigation of the Interaction of Two Richtmyer-Meshkov-unstable Gas Cylinders, in preparation, (2002).

Zoldi, C., A Numerical and Experimental Study of a Shock-accelerated Heavy Gas Cylinder, Ph.D. thesis, Department of Applied Mathematics, State University of New York at Stony Brook, (2002).

Zoldi, C., Personal communication, (2001).

Author Profile

Christopher Tomkins: He was educated in mechanical engineering at Georgia Tech (B.M.E., 1993) and at the University of Illinois at Urbana-Champaign (M.S., 1997), before earning his Ph.D. in Theoretical and Applied Mechanics at UIUC in 2000. His research interests involve the experimental investigation of complex fluid flows, including the use of high-resolution PIV to probe the structure of wall turbulence, and the investigation of unstable fluid interfaces. He currently holds a joint post-doctoral position at Los Alamos National Laboratory within the Physics (P) and Dynamic Experimentation (DX) Divisions.

Katherine Prestridge: She is a technical staff member at Los Alamos National Laboratory in the Dynamic Experimentation Division. She works on experiments to better understand the physics of fluid instabilities and particle transport in shock-accelerated and explosively-driven flows. She received her Ph.D. in Mechanical Engineering from the University of California at San Diego in 1998, and her B.S. in Aerospace Engineering from Princeton University in 1992.

Paul Rightley: He has been employed at Los Alamos National Laboratory in the Dynamic Experimentation Division since 1995 where he investigates high-speed transient phenomena including shock-driven fluid instabilities and surface friction in impacts. He moved to LANL upon receiving a Ph.D. in Engineering Sciences (Mechanical Engineering) from the University of California, San Diego studying multiphase flows. Before graduate school, he worked in the Propulsion and Thermophysics group at General Dynamics' Convair Division. He received his undergraduate engineering degree from New Mexico State University.

Peter Vorobieff: He is an experimental fluid dynamicist with an applied mathematics background. His primary research interests are hydrodynamic instabilities and transition to turbulence. He received his Ph.D. in Mechanical Engineering in 1996 (Lehigh University, Pennsylvania). Presently he is an Assistant Professor at the University of New Mexico. His current research involves wake and shock-driven instabilities.

Robert Benjamin: He is a Laboratory Fellow at Los Alamos, where he has been on the research staff for 28 years. He has done experimental research in fluid instability, high-speed diagnostics and inertial confinement fusion. He earned a B.S. in Engineering Physics at Cornell University and a Ph.D. in physics at MIT. He recently published a book for precollege students about fluid instabilities, entitled Spills and Ripples.